Phenotyping of multiple sclerosis lesions according to innate immune cell activation using TSPO-PET

Marjo Nylund[1,2,3], Marcus Sucksdorff[1,2,3], Markus Matilainen[1,4], Eero Polvinen[1,2,3], Jouni Tuisku[1] and Laura Airas[1,2,3,5]

[1] Turku PET Centre, Turku, Finland
[2] Clinical Neurosciences, University of Turku, Turku, Finland
[3] Neurocenter, Turku University Hospital, Turku, Finland
[4] Faculty of Science and Engineering, Åbo Akademi University, Turku, Finland
[5] Department of Neurology, Yale School of Medicine, New Haven, CT, USA

Correspondence to Laura Airas
Turku PET Centre, Turku University Hospital and University of Turku
Po Box 52, 20521 Turku, Finland
E-mail: laura.airas@utu.fi

Running title: MS lesion phenotyping with TSPO-PET

ACCEPTED MANUSCRIPT

Downloaded from https://academic.oup.com/braincomms/advance-article/doi/10.1093/braincomms/fcab301/6479693 by Turun Yliopiston Kirjasto user on 04 January 2022

© The Author(s) 2021. Published by Oxford University Press on behalf of the Guarantors of Brain.
This is an Open Access article distributed under the terms of the Creative Commons Attribution License (https://creativecommons.org/licenses/by/4.0/), which permits unrestricted reuse, distribution, and reproduction in any medium, provided the original work is properly cited.

ABSTRACT

Chronic active lesions are promotors of neurodegeneration and disease progression in multiple sclerosis. They harbour a dense rim of activated innate immune cells at the lesion edge, which promote lesion growth and thereby induce damage. Conventional MRI is of limited help in identifying the chronic active lesions, so alternative imaging modalities are needed. Objectives were to develop a PET-based automated analysis method for phenotyping of chronic lesions based on lesion-associated innate immune cell activation and to comprehensively evaluate the prevalence of these lesions in the various clinical subtypes of multiple sclerosis, and their association with disability.

In this work we use TSPO-PET-imaging for phenotyping chronic multiple sclerosis lesions at large scale. For this, we identified 1510 white matter T1-hypointense lesions from 91 multiple sclerosis patients [67 relapsing-remitting, 24 secondary progressive]. Innate immune cell activation at the lesion rim was measured using PET-imaging and the TSPO-binding radioligand ^{11}C-PK11195. A T1-hypointense lesion was classified as rim-active if the distribution volume ratio of ^{11}C-PK11195-binding was low in the plaque core and considerably higher at the plaque edge. If no significant ligand-binding was observed, the lesion was classified as inactive. Plaques that had considerable ligand-binding both in the core and at the rim were classified as overall-active. Conventional MRI and disability assessment using Expanded Disability Status Scale were performed at the time of PET-imaging. In the secondary progressive cohort, an average of 19 % (median, interquartile range 11-26) of T1 lesions were rim-active in each individual patient, compared to 10 % (interquartile range 0-20) among relapsing remitting patients (P = 0.009). Secondary progressive patients had a median of 3 (range 0-11) rim-active lesions, vs. 1 (range 0-18) among relapsing remitting patients (P = 0.029). Among those patients who had rim-active lesions (n = 63) the average number of active voxels at the rim was higher among secondary progressive compared to relapsing remitting patients (median 158 versus 74; P = 0.022). The number of active voxels at the rim correlated significantly with Expanded Disability Status Scale (R=0.43, P <0.001), and the volume of the rim-active lesions similarly correlated with Expanded Disability Status Scale (R=0.45, P < 0.001).

Our study is the first to report *in vivo* phenotyping of chronic lesions at large scale, based on TSPO-PET. Patients with higher disability displayed a higher proportion of rim-active lesions.

ACCEPTED MANUSCRIPT

Downloaded from https://academic.oup.com/braincomms/advance-article/doi/10.1093/braincomms/fcab301/6479693 by Turun Yliopiston Kirjasto user on 04 January 2022

The *in vivo* lesion phenotyping methodology offers a new tool for individual assessment of smouldering (rim-active) lesion burden.

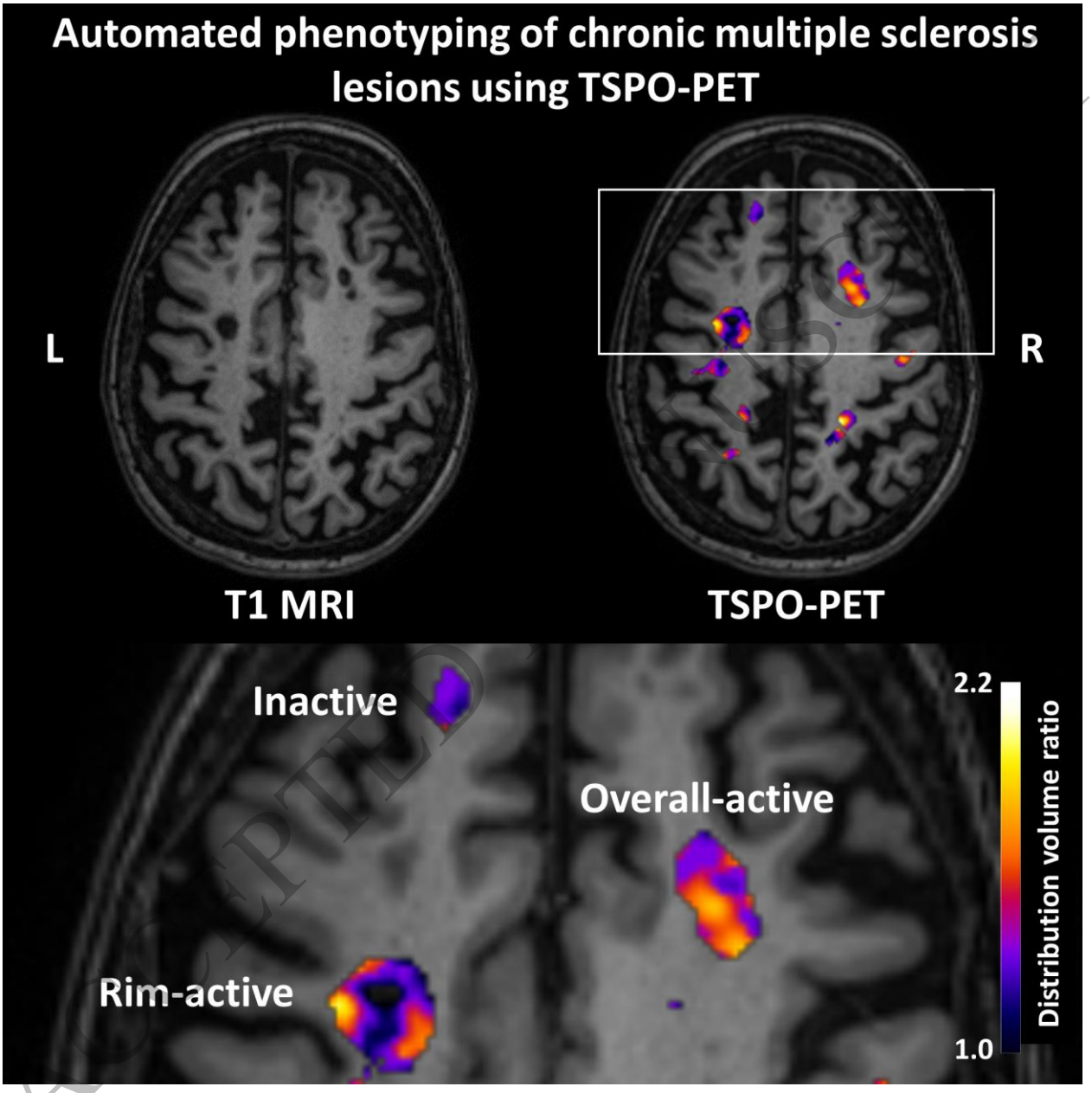

Graphical Abstract
165x165 mm (0.2 x DPI)

Keywords: PET-imaging; TSPO; Multiple sclerosis; Innate immune cell; White matter lesions

Downloaded from https://academic.oup.com/braincomms/advance-article/doi/10.1093/braincomms/fcab301/6479693 by Turun Yliopiston Kirjasto user on 04 January 2022

Abbreviations:

BP_{ND} = Binding potential, cMRI = conventional MRI, DVR = distribution volume ratio, EDSS = expanded disability status scale, HC = healthy control, HRRT = High-Resolution Research Tomograph, IQR = Interquartile range, LST = Lesion Segmentation Tool, MNI = Montreal Neurological Institute database, MSSS = Multiple Sclerosis Severity Score, MS = multiple sclerosis, NAWM = normal appearing white matter, ROI = Region of interest, RRMS = relapsing remitting multiple sclerosis, SD = standard deviation, SPMS = secondary progressive multiple sclerosis, TSPO = translocator protein

ACCEPTED MANUSCRIPT

Downloaded from https://academic.oup.com/braincomms/advance-article/doi/10.1093/braincomms/fcab301/6479693 by Turun Yliopiston Kirjasto user on 04 January 2022

INTRODUCTION

Despite appropriate use of disease modifying therapies, the majority of relapsing-remitting multiple sclerosis (RRMS) patients proceed to secondary progressive disease course characterized by gradual accumulation of disability and paucity of relapses.[1] In secondary progressive multiple sclerosis (SPMS), immune cell trafficking from the periphery is reduced and neuropathological studies reveal chronic and compartmentalized activation of the innate immune system within the CNS behind an intact blood-brain-barrier, and fewer active focal lesions.[2] In clinical imaging, this translates to fewer MRI-detectable acute gadolinium-enhancing plaques and more abundant chronic T1 hypointense lesions. In secondary progressive multiple sclerosis, the predominant lesion type in neuropathological studies is a chronic lesion. These typically have an acellular lesion core, and lesion edge not containing (inactive) or containing activated microglial cells and macrophages (chronic active i.e. smouldering plaques).[3,4] The smouldering lesions are frequently associated with signs of axonal damage and demyelination.[5] The smouldering lesion-associated innate immune cells have a proinflammatory phenotype and increased iron-uptake,[6] which makes them visible *in vivo* by MR sequences sensitive to tissue susceptibility.[7] Clinical imaging studies have recently identified the iron rim lesions as a marker of poor prognosis, with associated lesion growth and more rapid clinical disease progression.[8-10] Depending on the study, the iron rim lesion fraction has varied between 0 -75 % per patient.[8,9,11-13]

PET-imaging using radioligands binding to the 18-kD translocator protein (TSPO) has similarly been used to specifically quantitate innate immune cell activation *in vivo*, and increased PET-detectable TSPO-expression in lesions with paramagnetic rims has been demonstrated.[13] TSPO-PET signal is stronger both in the normal appearing white matter (NAWM) and in the perilesional area of SPMS patients compared to RRMS patients and controls[14-19] and upon longitudinal follow-up, an increase in TSPO-binding in the NAWM was observed in an untreated group of multiple sclerosis patients studied using PET.[20] In lesional areas of multiple sclerosis brain, gadolinium-enhancing lesions have strong TSPO-ligand accumulation,[21] whereas non-enhancing T2 lesions have more variable TSPO-binding patterns both within the lesion and in the perilesional area.[16,22] There is yet no comprehensive *in vivo* PET-based analysis of innate

ACCEPTED MANUSCRIPT

Downloaded from https://academic.oup.com/braincomms/advance-article/doi/10.1093/braincomms/fcab301/6479693 by Turun Yliopiston Kirjasto user on 04 January 2022

immune cell activity at the chronic lesion rim. It would be advantageous to be able to define the frequency of smouldering lesions at different stages of the disease, to better understand their impact on disease progression, to shed light to the risk of progression and disability accrual, and to be able to measure more accurately the impact the innate immune system-modifying therapies within the CNS *in vivo*.

The aim of this study was to develop an automated TSPO-PET analysis method for comprehensive phenotyping of individual chronic lesions based on their microglial activation status *in vivo*. Using this method we determined the proportions of different lesion types in various multiple sclerosis cohorts, the prevalence of chronic active lesions at individual patient level, and demonstrated that a higher proportion of lesions with innate immune cell activity at the lesion rim was associated with increased clinical disease severity.

MATERIALS AND METHODS

Study subjects

A total of 91 multiple sclerosis patients were imaged. Of them 67 had RRMS and 24 had SPMS. For comparison, 18 age- and sex-matched healthy control persons were included. The patients were recruited from the outpatient clinic of the Division of Clinical Neurosciences at the University Hospital of Turku, Finland. The requirement for inclusion were willingness to participate in a PET study and multiple sclerosis diagnosis according to McDonald criteria 2017.[23] All participants provided written informed consent and the study was conducted according to the Declaration of Helsinki, with approval by the Ethics Committee of the Hospital District of Southwest Finland.

Clinical relapse and/or corticosteroid treatment within 30 days of evaluation, and gadolinium contrast enhancement in conventional MRI (cMRI) were considered as exclusion criteria in order to avoid confounding effects of acute inflammation on the innate immune cell activation and chronic lesion characterization. Exclusion criteria also included inability to tolerate PET or cMRI, current pregnancy, active neurological or autoimmune disease other than multiple sclerosis or another comorbidity considered significant. The disease severity was evaluated by

ACCEPTED MANUSCRIPT

Downloaded from https://academic.oup.com/braincomms/advance-article/doi/10.1093/braincomms/fcab301/6479693 by Turun Yliopiston Kirjasto user on 04 January 2022

experienced clinicians using Expanded Disability Status Scale (EDSS) score and a standardized examination form, the Neurostatus (neurostatus.net).

MRI acquisition, MRI data analysis, and creation of individual lesion core and rim ROIs

cMRI with a 3-T Ingenuity TF PET/MR scanner (Philips) was performed for the evaluation of multiple sclerosis pathology and for the acquisition of anatomic reference for the PET images. cMRI sequences were as previously described.[24] A semi-automated method was used first to create combined T2 lesion region of interest (ROI) mask image using the Lesion Segmentation Tool (LST, www.statistical-modelling.de/lst.html, a toolbox running in SPM8)[25] and Carimas (https://turkupetcentre.fi/carimas/) for manual editing as described previously.[19] A combined T1 lesion ROI mask image was manually shaped slice by slice. The resulting T1 lesion ROI mask image was used to fill the corresponding T1 image with the lesion-filling tool in LST. The filled T1 was then used for segmenting grey matter, white matter and thalamus with Freesurfer 5.3 software (http://surfer.nmr.mgh.harvard.edu/). Total T1 lesion load was measured from the manually edited T1 ROI masks. Individual T1 lesion core ROI masks were created by separation of individual lesions from the combined T1 lesion masks. Lesions $\leq$ 27 mm^3 in size were excluded to avoid inclusion of unspecific T1 hypointensities. This resulted with a total of 1857 T1 lesions (Fig. 1A).

The 2 mm lesion rim ROI was created by dilating the T1 lesion core ROI by two voxels from the lesion edge, and then removing the lesion core ROI (Fig. 1A). This resulted with a lesion rim ROI of width of two voxels extending out from the T1 lesion edge. The 3 mm perilesional ROI was created similarly by dilating the T1 lesion core ROI mask image by three voxels from the T1 lesion edge and then removing the lesion core ROI from the resulting image. In addition, NAWM ROI was created by removing the combined T2 lesion ROI from the white matter ROI. Of the 1857 T1 hypointensities larger than 27 mm^3 size, 347 were discarded (those with less than 75 % of the lesion volume in the white matter, those with $\leq$ 27 mm^3 of the rim in the white matter and lesions in the cerebellum and brain stem). This resulted with 1510 lesions for the final evaluation (Fig. 1A). The pre-selection of lesions according to location was done to ensure good

ACCEPTED MANUSCRIPT

Downloaded from https://academic.oup.com/braincomms/advance-article/doi/10.1093/braincomms/fcab301/6479693 by Turun Yliopiston Kirjasto user on 04 January 2022

quality PET analysis, given that the High-Resolution Research Tomograph (HRRT) PET scanner resolution is 2.5 mm, and to avoid any potential disturbance related to infratentorial artefacts.

PET image acquisition

The radiochemical synthesis of ^{11}C-PK11195 has been previously described by Rissanen et al. 2018.[19] The mean injected dose was 476 ± 52 MBq (mean ± standard deviation, SD) for the multiple sclerosis patient group and 490 ± 16 MBq for the healthy control group with no significant dose differences between the groups. PET scan was performed using a brain-dedicated ECAT HRRT scanner (CTI/Siemens) with an intrinsic spatial resolution of 2.5 mm. Sixty minute dynamic PET scan was started simultaneously with intravenous bolus injection of the ^{11}C-PK11195 radioligand. Prior the ligand infusion, a 6-min transmission scan for attenuation correction was obtained using a 137Cs point source. Thermoplastic head mask was used to minimize the movement.

PET image post-processing and analysis

PET images were reconstructed using 17 time frames as described previously.[19] The reconstructed PET images were smoothed using a Gaussian 2.5-mm post-reconstruction filter.[16,19] Possible displacements between frames were corrected using mutual information realignment in SPM8. Finally PET images were coregistered to T1 MRI and resampled to match the MRI voxel size 1 x 1 x 1 mm^3. Innate immune cell activation was evaluated as specific binding of ^{11}C-PK11195 using distribution volume ratio (DVR) in pre-specified ROIs. For the estimation of the ^{11}C-PK11195 DVR, the time–activity curve corresponding to a reference region devoid of specific TSPO-binding was acquired for each PET session using a supervised cluster algorithm with four predefined kinetic tissue classes (SuperPK software).[26,27] The reference tissue–input Logan method with a time interval from 20 to 60 min, was applied to the regional time–activity curves using the supervised cluster algorithm grey reference input. For the individual lesion DVR analysis the voxel-wise parametric binding potential (BP_{ND}) maps were calculated using basis function implementation of SRTM14 with 250 basis functions. Lower and upper bounds for theta were set to 0.06 1/min and 0.8 1/min. The resulting parametric maps were

ACCEPTED MANUSCRIPT

Downloaded from https://academic.oup.com/braincomms/advance-article/doi/10.1093/braincomms/fcab301/6479693 by Turun Yliopiston Kirjasto user on 04 January 2022

normalized to MNI space (Montreal Neurological Institute database) in SPM8 and the BP_{ND} images were transformed to DVR (DVR = BP_{ND} +1).

Individual lesion evaluation for innate immune cell activation

The mean DVR ± SD of all white matter voxels was calculated from all individual DVR images of healthy control subjects (HC; n = 18). Thereafter, 95% confidence interval threshold (HC mean + 1.96*SD) was used to describe anomalously high voxel activity in lesion phenotyping. Consequently, for each subject, binary TSPO-active voxels were characterized from the DVR images exceeding this threshold (DVR value of 1.56 in our data). Clusters below three connected voxels were excluded in the TSPO-activity image for preventing the inclusion of random peak values.

The proportion of the active voxels in the lesion core ROI and at the rim ROI was used to classify lesions into three subtypes. 1) Rim-active lesion: lesions with less than 5 % active voxels in the core and at least 5 %-point higher proportion of active voxels at the rim compared to the core and lesions which have 5 - 20 % active voxels in the core and at the same time at least double the proportion of active voxels at the rim 2) inactive lesions: lesions with no active voxels at the rim or in the core 3) overall-active lesions: lesions which do not fit into the other two categories (Fig. 1A-B).

Statistical analysis

The statistical analyses were performed using R (version 4.0.3). Variables are reported as median (interquartile range, IQR) unless otherwise stated. Wilcoxon rank-sum test was used to assess the differences in DVRs, counts, proportions, volumes, and volume proportions between the two different groups. Spearman correlation coefficients were calculated in order to evaluate the relationships between the continuous variables. Fisher's exact test was used to compare the gender distributions between two groups and to compare distributions of plaque types in different group variables. EDSS was used to classify patients into two groups: < 4 and ≥ 4. The relationships between the volume of the rim-active lesions and EDSS and brain volume were modelled using multiple linear regression with EDSS and brain volume as outcome variables.

ACCEPTED MANUSCRIPT

Downloaded from https://academic.oup.com/braincomms/advance-article/doi/10.1093/braincomms/fcab301/6479693 by Turun Yliopiston Kirjasto user on 04 January 2022

Multiple linear regression model was used to assess contribution of rim-active lesion load to brain volume and EDSS. Gender, age, therapy, disease duration and rim-active lesion volume were used as predictive variables in all regression models. Disease modifying therapy at the time of PET scanning or at most 2 months before were categorized into two classes.[28] Rim-active lesion volume was included as its logarithm to make the models valid considering the assumptions of the multiple linear regression. All tests were two-tailed and a *P*-value less than 0.05 was considered statistically significant for all analyses.

Data availability

Anonymised data not published within the article will be shared over the next 3 years upon request from a qualified investigator.

RESULTS

The clinical demographic and radiographic data are given in Table 1. Of the 91 patients included, 67 (74 %) had RRMS and they were younger, had shorter disease duration and lower EDSS and Multiple Sclerosis Severity Score (MSSS) compared to those with secondary progressive disease (n = 24, 26 %). The mean age of all patients was 44.9 ± 9.7 years (mean ± SD) and their disease duration was 12.5 (± 7.7) years. Their median EDSS was 3.0 (IQR 2.0 - 3.5) and median MSSS was 3.9 (2.39 - 5.20). In addition to disease type comparison, patients were divided into two groups based on their EDSS. Those with EDSS 4 or higher (n = 22, 24 %) were older and had longer disease duration compared to those with EDSS < 4 (n= 69, 76 %).

Brain ^{11}C-PK11195 binding in multiple sclerosis patients and in healthy controls

^{11}C-PK11195 radioligand binding in the white matter of healthy controls was significantly lower (1.19 ± 0.04) compared to the NAWM of all multiple sclerosis patients (1.22 ± 0.05; $P = 0.014$) or SPMS patients separately (1.26 ± 0.06; $P < 0.001$). The innate immune cell activation was higher in SPMS patients compared to RRMS patients both in the NAWM (1.26 ± 0.06 vs. 1.21 ± 0.05, $P < 0.001$) and in the 0-3 mm perilesional area surrounding lesions (1.23 ± 0.07 vs. 1.19 ±

ACCEPTED MANUSCRIPT

Downloaded from https://academic.oup.com/braincomms/advance-article/doi/10.1093/braincomms/fcab301/6479693 by Turun Yliopiston Kirjasto user on 04 January 2022

0.08, P = 0.024). The DVR values within the combined T1 lesion ROI or at the combined T1 rim ROI were similar among the disease subtypes (Fig. 2).

Association of brain volumetric parameters and innate immune cell activation with clinical disability

Smaller whole brain and NAWM volume and higher T1 lesion load were significantly associated with higher clinical disability measured using EDSS (Fig. 3A-C). Higher DVR in the NAWM associated with both higher EDSS (R = 0.41, P < 0.001) and MSSS (R = 0.28, P = 0.0083; Fig. 3D-E). Higher DVR value in the 0-3 mm perilesional area correlated with EDSS (R = 0.21, P = 0.044; Fig. 3F) but no correlations were observed between the combined T1 rim ROI or the combined T1 lesion ROI DVRs and EDSS values (Fig. 3G-H).

Distribution of lesions according to innate immune cell activation at rim

Of the 1510 lesions in the final analysis, 246 (16 %) were rim-active lesions with a total lesion load of 96 cm^3 and 493 (33 %) were inactive lesions, 43 cm^3. Overall-active lesions (n = 771, 51 %) that do not fit into the other two categories had the largest total lesion load of 371 cm^3 (Fig. 1A). The average (±SD) number of rim-active lesions per patient was 2.7 ± 3.3 [median 2, IQR 0 - 4, range 0 - 18)]. 28 patients (31 %) did not have rim-active lesions. The average number of inactive lesions was 5.4 ± 4.0 [median 5, IQR 2.5 - 7.5, range 0-22)]. Six patients (7 %) had no inactive lesions (Table 2). Nearly all patients (96 %) had overall-active lesions (Table 2). The average number of overall-active lesions per patients was 8.5 ± 7.7 [median 6, IQR 3-11.5, range 0-34)].

Distribution of lesion phenotypes according to clinical patient profile

Among SPMS patients the number of rim-active lesions (median 3, IQR 1-4, range 0-11) was higher compared to RRMS patients (median, 1 IQR 0 - 3, range 0 - 18, P = 0.029; Table 2). In an individual SPMS patient 19 % of T1 lesions were rim-active, 27 % were inactive and 51 % were overall-active. In RRMS 10 % of lesions were rim-active, 40 % were inactive and 47 % were overall-active. The fractions of rim-active and inactive lesions between SPMS and RRMS were

ACCEPTED MANUSCRIPT

Downloaded from https://academic.oup.com/braincomms/advance-article/doi/10.1093/braincomms/fcab301/6479693 by Turun Yliopiston Kirjasto user on 04 January 2022

statistically significantly different (P = 0.009 and P = 0.029, respectively; Table 2). The total T1 lesion load per patient was significantly higher in SPMS [7.20 cm^3 (4.04 - 16.0)] compared to RRMS [1.77 cm^3 (0.77-3.29), P < 0.001]. Similarly, the average volume of rim-active lesions per patient was larger among SPMS patients [0.41 cm^3 (0.15-3.18)] compared to relapsing-remitting [0.06 cm^3 (0 - 0.25), P < 0.001]. Of the total lesion volume among SPMS patients, 13 % belonged to rim-active lesion fraction and 4.9 % belonged to inactive lesion fraction, whereas in relapsing-remitting patients the corresponding proportions were 2.4 % and 23 %, respectively (P = 0.001 and P = 0.002; Table 2). There were no differences in the volume percentages of overall-active lesions between the multiple sclerosis subgroups. Similar results were obtained when the patients were subdivided based on EDSS (EDSS ≥ 4 or < 4, Table 2).

The frequencies of the different plaque types were statistically significantly different between patients with EDSS ≥ 4 and EDSS < 4 when evaluated using the Fisher's exact test (P < 0.001; Fig.4A). In the patient cohort with EDSS ≥ 4 the fraction of rim-active lesions was higher (56 %) and fraction of inactive lesions was lower (24 %) compared to patients with EDSS < 4 (49 % and 37 %, respectively). Similar trend was observed between SPMS and RRMS, but statistical significance was not reached (Fig. 4B). Distributions of volume percentages across the lesion subtypes were different both in EDSS ≥ 4 vs. EDSS < 4 and SPMS vs. RRMS (P < 0.001, Fig. 4C-D).

Correlation of rim-active lesion load with clinical disability and brain atrophy

Higher rim-active lesion volume correlated with higher EDSS (R = 0.45, P < 0.001; Fig. 5A) and with lower brain volume (R = -0.26, P = 0.041; Fig. 5B) among the 63 individuals who had rim-active lesions. In the entire cohort, higher number of rim-active lesions correlated with higher EDSS (R = 0.31, P = 0.003, data not shown). The rim-active lesion associations with higher clinical disability (P < 0.001) and brain atrophy (P = 0.043) remain significant when taking into account background variables gender, age, therapy and disease duration in multiple linear regression.

ACCEPTED MANUSCRIPT

Downloaded from https://academic.oup.com/braincomms/advance-article/doi/10.1093/braincomms/fcab301/6479693 by Turun Yliopiston Kirjasto user on 04 January 2022

Innate immune cell activation at rim is variable but more prevalent among patients with advanced disease

The average active voxel number at the rim-active rim per patient was 92 (median; IQR 47 - 203), and on average there were significantly more active voxels at the rim in SPMS patients compared to RRMS (medians 158 vs. 74, P = 0.022; Fig. 6A, Table 2). Similarly, there was a significantly higher number of active voxels at the rim in patients with EDSS ≥ 4 vs. EDSS < 4 (medians 210 vs. 73, P = 0.003; Fig. 6B, Table 2). Number of active voxels at rim correlated significantly both with EDSS (R = 0.43, P < 0.001) and MSSS (R = 0.31, P = 0.013; Fig. 6C-D).

The lesion sizes varied greatly within this heterogeneous cohort of multiple sclerosis patients. The smallest lesion (inactive, 0.028 cm^3 in volume) had 69 voxels at the rim and the largest lesion (20.2 cm^3 in volume) had 20862 voxels at the rim. This largest lesion was rim-active with 2205 (11 %) active voxels at the rim. The smallest rim-active lesion (0.028 cm^3) had 109 voxels at the rim, with eight active voxels (7 %; Fig. 6E). The proportion of active voxels at the rim of rim-active lesions varied greatly, between 5 % and 45 % (Fig. 6E).

DISCUSSION

The results from this comprehensive, cross-sectional study focusing on 91 PET-imaged multiple sclerosis patients and 1510 lesions demonstrate that *in vivo* TSPO-PET can be used to quantify innate immune cell activation at chronic lesion edge with subsequent categorization of the lesions into rim-active and inactive lesions. At patient level, the rim-active lesion fraction was larger among SPMS (19 %) compared to RRMS (10 %) and according to multiple linear regression modelling, the rim-active lesion load contributed more significantly to clinical disability (P = 0.014) than NAWM DVR (P = 0.6; data not shown). The detrimental nature of the rim-active lesions was demonstrated by correlation of rim-active lesion load at rim to brain atrophy measures in MRI. Similarly, patients with increased disability, older age and longer disease duration had proportionately more rim-active than rim-inactive lesions and a significant difference was observed in the perilesional microglial activation between RRMS and SPMS patients.[19] Moreover, higher TSPO binding in the perilesional NAWM predicted progression during a 4-year follow-up.[29] In CNS disease the innate immune system may respond to neuronal

ACCEPTED MANUSCRIPT

Downloaded from https://academic.oup.com/braincomms/advance-article/doi/10.1093/braincomms/fcab301/6479693 by Turun Yliopiston Kirjasto user on 04 January 2022

injury by activation.[30] On the other hand, the innate immune system may get arrested in a proinflammatory, neuronal damage promoting phenotype once activated in the context of neuroinflammatory disease. In multiple sclerosis this may promote a state of self-propagating damage contributing to disease progression and disability accrual.[30] In line with this, microglial activation in the NAWM was recently shown to co-localize with markers of microstructural damage in an *in vivo* study combining TSPO-PET and DTI-MRI imaging.[24] In addition, microglial activation has been shown to associate with age and with MS disease duration.[19,31,32] Due to this phenomenon, we took age and disease duration into account in the model where the rim active lesion load association with clinical disability and brain atrophy was addressed (Fig. 5).

In the seminal neuropathology work by Frischer et al,[4] out of 2476 white matter plaques, 35 % were classified as active plaques and were majorly found only in relapsing-remitting multiple sclerosis patients. 15 % of the lesions were smouldering and almost exclusively found in progressive multiple sclerosis. Of the lesions 35 % were inactive and 15 % were classified as shadow plaques. In the present work, the lesion distribution was very similar with 16 % rim-active (corresponding to smouldering), 33 % inactive lesions and 51 % overall-active (likely partly corresponding to the pathological classification of active plaques and shadow plaques). In both studies the average disease duration was 12 years. In the Frischer analysis half of the lesions were infratentorial, and the plaque type distribution was found to be rather similar between supratentorial and infratentorial lesions. In the present work all evaluated lesions were supratentorial white matter lesions.

TSPO-PET detects both activated microglial cells and macrophages. In addition, a small proportion (25 %) of astrocytes bind the TSPO-ligands.[33] It is thus impossible to determine for certain the exact cellular correlates of the increased TSPO-binding, but a most likely interpretation of our results is that the ligand binding at chronic lesion edge and in the NAWM reflect proinflammatory microglia and macrophage activation with some binding to astrocytes.[34,35] The lesions with increased TSPO binding both in the core and at rim have possibly evolved more recently.[6,36] The use of novel PET-ligands may assist in more accurate *in vivo* segregation of astrocytes from microglial cells, or M1-type innate immune cells from M2-

ACCEPTED MANUSCRIPT

Downloaded from https://academic.oup.com/braincomms/advance-article/doi/10.1093/braincomms/fcab301/6479693 by Turun Yliopiston Kirjasto user on 04 January 2022

type innate immune cells, and thus may further improve the specificity of the *in vivo* plaque differentiation in the future.[37,38]

MRI-based techniques which rely on detection of iron within activated microglia and macrophages have been developed to identify chronic active or smouldering lesions *in vivo*.[8,9,11,39-44] Here, MR sequences sensitive to tissue susceptibility due to paramagnetic properties of the cells such as high-resolution T2*, susceptibility-weighted imaging (SWI), phase MRI using 7T or 3T, and quantitative susceptibility mapping (QSM) have been used.[8,9,11,13,39-45] Iron rim lesions were detected in 46 - 81 % of the studied multiple sclerosis patients depending on the cohort/study.[10,42,46-49] Unlike the neuropathological studies,[4,50,51] some [11,13,46] but not all[52] MRI-studies of iron rim lesions have detected them more often in RRMS patients compared to progressive multiple sclerosis. Larger MRI studies with more homogeneous methodologies regarding iron rim detection will likely help settle this discrepancy. The smouldering lesions are potentially the ones to expand.[10,46,53] Our data are in line with this, as in our cohort the largest lesions were rim-active, were often located in the periventricular area, and had likely been formed by fusion of several rim-active lesions together, with the largest such confluent lesion having a volume of 20.2 cm^3. On the contrary, the largest inactive lesion was only 1.3 cm^3.

The analysis of hot microglia at rim using TSPO-PET-imaging relies on fully automated, quantitative methodology and allows sensitive detection of the detrimental cell clusters in a three-dimensional space. In this study a novel approach was used to define the rim as two voxels extending from the T1 lesion edge with the idea to address as limited rim area as possible with taking the resolution of PET scanner into account. In our previous work the DVR in the 0-6 mm perilesional ROI was different in SPMS vs RRMS.[19] In the present work 0-3 mm perilesional ROI was similarly different in RRMS vs SPMS, but in the 2 mm perilesional ROI no difference was observed (Fig. 2C and 2D). We interpret that the latter is perhaps due to the close vicinity of the lesion core with lower DVR and no differences between RRMS and SPMS. All hemispheric white matter T1 lesions with minimum rim and core size of >27 mm^3 were included unless they extended to the grey matter by more than 25 %. In some of the MRI studies only well-demarcated independent lesions have been included in the analysis,[46] which might have promoted the predominance of iron-rim lesions in earlier disease stages. Despite the differences

ACCEPTED MANUSCRIPT

Downloaded from https://academic.oup.com/braincomms/advance-article/doi/10.1093/braincomms/fcab301/6479693 by Turun Yliopiston Kirjasto user on 04 January 2022

in the methodologies between MRI and PET, the frequency of the rim-active lesions in the present study, with 16 % of all lesions being rim-active in the entire multiple sclerosis cohort, was in a similar range compared to many of the MRI studies.

Taken together, there are now neuropathology-based, susceptibility MRI-based and TSPO-PET-based methods to quantify progression-associated smouldering inflammation in multiple sclerosis brain. Future studies will demonstrate how the different methods can be used in a complementary way to evaluate the dynamic innate inflammatory process contributing to neuroaxonal damage and disease progression. Accurate and dynamic *in vivo* assessment of progression-related innate immune system activation has potential to advance our understanding of the mechanisms related to disability accrual among multiple sclerosis patients. This has implications for predicting future disease course,[29] for obtaining meaningful outcome markers and for selecting optimal patients when performing treatment trials of progressive multiple sclerosis.

Acknowledgements

We thank all multiple sclerosis patients participating in this study, and the expert personnel of the Turku PET Centre.

Funding

This work was funded by the Academy of Finland, the Sigrid Juselius foundation, the Finnish MS Foundation, the Finnish Medical Foundation and the InFLAMES Flagship Programme of the Academy of Finland (decision number: 337530) .

Competing interests

Marcus Sucksdorff has served on advisory boards for Sanofi-Aventis and Roche, and has received speaker honoraria from Merck Serono and travel honoraria Orion, Roche, Biogen and Sanofi-Aventis and received research support from The Finnish Medical Foundation, The Finnish MS Foundation and from The Finnish Medical Society (Finska Läkaresällskapet)

ACCEPTED MANUSCRIPT

Downloaded from https://academic.oup.com/braincomms/advance-article/doi/10.1093/braincomms/fcab301/6479693 by Turun Yliopiston Kirjasto user on 04 January 2022

Laura Airas has received honoraria from Biogen, Roche, Genzyme, Merck Serono and Novartis, and institutional research grant support from Finnish Academy, Sanofi-Genzyme and Merck Serono.

References

1. Correale J, Gaitán MI, Ysrraelit MC, Fiol MP. Progressive multiple sclerosis: from pathogenic mechanisms to treatment. *Brain*. Mar 2017;140(3):527-546. doi:10.1093/brain/aww258
2. Lassmann H. Mechanisms of White Matter Damage in Multiple Sclerosis. *Glia*. Nov 2014;62(11):1816-1830. doi:10.1002/glia.22597
3. Kutzelnigg A, Lucchinetti CF, Stadelmann C, et al. Cortical demyelination and diffuse white matter injury in multiple sclerosis. *Brain*. Nov 2005;128(Pt 11):2705-12. doi:10.1093/brain/awh641
4. Frischer JM, Weigand SD, Guo Y, et al. Clinical and pathological insights into the dynamic nature of the white matter multiple sclerosis plaque. *Ann Neurol*. Nov 2015;78(5):710-21. doi:10.1002/ana.24497
5. Frischer JM, Bramow S, Dal-Bianco A, et al. The relation between inflammation and neurodegeneration in multiple sclerosis brains. *Brain*. May 2009;132(5):1175-89. doi:10.1093/brain/awp070
6. Gillen KM, Mubarak M, Nguyen TD, Pitt D. Significance and In Vivo Detection of Iron-Laden Microglia in White Matter Multiple Sclerosis Lesions. *Front Immunol*. 2018;9:255. doi:10.3389/fimmu.2018.00255
7. Wang Y, Liu T. Quantitative susceptibility mapping (QSM): Decoding MRI data for a tissue magnetic biomarker. *Magn Reson Med*. Jan 2015;73(1):82-101. doi:10.1002/mrm.25358
8. Dal-Bianco A, Grabner G, Kronnerwetter C, et al. Slow expansion of multiple sclerosis iron rim lesions: pathology and 7 T magnetic resonance imaging. *Acta Neuropathol*. 01 2017;133(1):25-42. doi:10.1007/s00401-016-1636-z
9. Absinta M, Sati P, Schindler M, et al. Persistent 7-tesla phase rim predicts poor outcome in new multiple sclerosis patient lesions. *J Clin Invest*. 07 2016;126(7):2597-609. doi:10.1172/JCI86198
10. Absinta M, Sati P, Masuzzo F, et al. Association of Chronic Active Multiple Sclerosis Lesions With Disability In Vivo. *JAMA Neurol*. Aug 2019;doi:10.1001/jamaneurol.2019.2399
11. Mehta V, Pei W, Yang G, et al. Iron is a sensitive biomarker for inflammation in multiple sclerosis lesions. *PLoS One*. 2013;8(3):e57573. doi:10.1371/journal.pone.0057573
12. Blindenbacher N, Brunner E, Asseyer S, et al. Evaluation of the 'ring sign' and the 'core sign' as a magnetic resonance imaging marker of disease activity and progression in clinically isolated syndrome and early multiple sclerosis. *Mult Scler J Exp Transl Clin*. 2020 Jan-Mar 2020;6(1):2055217320915480. doi:10.1177/2055217320915480
13. Kaunzner UW, Kang Y, Zhang S, et al. Quantitative susceptibility mapping identifies inflammation in a subset of chronic multiple sclerosis lesions. *Brain*. 01 2019;142(1):133-145. doi:10.1093/brain/awy296
14. Banati RB, Newcombe J, Gunn RN, et al. The peripheral benzodiazepine binding site in the brain in multiple sclerosis: quantitative in vivo imaging of microglia as a measure of disease activity. *Brain*. Nov 2000;123 (Pt 11):2321-37. doi:10.1093/brain/123.11.2321

ACCEPTED MANUSCRIPT

Downloaded from https://academic.oup.com/braincomms/advance-article/doi/10.1093/braincomms/fcab301/6479693 by Turun Yliopiston Kirjasto user on 04 January 2022

15. Politis M, Giannetti P, Su P, et al. Increased PK11195 PET binding in the cortex of patients with MS correlates with disability. *Neurology*. Aug 2012;79(6):523-30. doi:10.1212/WNL.0b013e3182635645
16. Rissanen E, Tuisku J, Rokka J, et al. In Vivo Detection of Diffuse Inflammation in Secondary Progressive Multiple Sclerosis Using PET Imaging and the Radioligand ^{11}C-PK11195. *J Nucl Med*. Jun 2014;55(6):939-44. doi:10.2967/jnumed.113.131698
17. Datta G, Colasanti A, Kalk N, et al. C-PBR28 and. *J Nucl Med*. 09 2017;58(9):1477-1482. doi:10.2967/jnumed.116.187161
18. Vomacka L, Albert NL, Lindner S, et al. TSPO imaging using the novel PET ligand [*EJNMMI Res*. Oct 2017;7(1):89. doi:10.1186/s13550-017-0340-x
19. Rissanen E, Tuisku J, Vahlberg T, et al. Microglial activation, white matter tract damage, and disability in MS. *Neurol Neuroimmunol Neuroinflamm*. May 2018;5(3):e443. doi:10.1212/NXI.0000000000000443
20. Sucksdorff M, Tuisku J, Matilainen M, et al. Natalizumab treatment reduces microglial activation in the white matter of the MS brain. *Neurology-Neuroimmunology & Neuroinflammation*. Jul 2019;6(4)e574. doi:10.1212/nxi.0000000000000574
21. Debruyne JC, Van Laere KJ, Versijpt J, et al. Semiquantification of the peripheral-type benzodiazepine ligand C-11 PK11195 in normal human brain and application in multiple sclerosis patients. *Acta Neurologica Belgica*. Sep 2002;102(3):127-135.
22. Datta G, Colasanti A, Kalk N, et al. 11C-PBR28 and 18F-PBR111 Detect White Matter Inflammatory Heterogeneity in Multiple Sclerosis. *J Nucl Med*. Sep 2017;58(9):1477-1482. doi:10.2967/jnumed.116.187161
23. Thompson AJ, Banwell BL, Barkhof F, et al. Diagnosis of multiple sclerosis: 2017 revisions of the McDonald criteria. *Lancet Neurology*. Feb 2018;17(2):162-173. doi:10.1016/s1474-4422(17)30470-2
24. Bezukladova S, Tuisku J, Matilainen M, et al. Insights into disseminated MS brain pathology with multimodal diffusion tensor and PET imaging. *Neurol Neuroimmunol Neuroinflamm*. May 2020;7(3)doi:10.1212/NXI.0000000000000691
25. Schmidt P, Gaser C, Arsic M, et al. An automated tool for detection of FLAIR-hyperintense white-matter lesions in Multiple Sclerosis. *Neuroimage*. Feb 15 2012;59(4):3774-83. doi:10.1016/j.neuroimage.2011.11.032
26. Turkheimer FE, Edison P, Pavese N, et al. Reference and target region modeling of [11C]-(R)-PK11195 brain studies. *J Nucl Med*. Jan 2007;48(1):158-67.
27. Yaqub M, van Berckel BN, Schuitemaker A, et al. Optimization of supervised cluster analysis for extracting reference tissue input curves in (R)-[(11)C]PK11195 brain PET studies. *J Cereb Blood Flow Metab*. Aug 2012;32(8):1600-8. doi:jcbfm201259 [pii]
10.1038/jcbfm.2012.59
28. Scolding N, Barnes D, Cader S, et al. Association of British Neurologists: revised (2015) guidelines for prescribing disease-modifying treatments in multiple sclerosis. *Pract Neurol*. Aug 2015;15(4):273-9. doi:10.1136/practneurol-2015-001139
29. Sucksdorff M, Matilainen M, Tuisku J, et al. Brain TSPO-PET predicts later disease progression independent of relapses in multiple sclerosis. *Brain*. Oct 2020;doi:10.1093/brain/awaa275
30. Perry VH, Nicoll JAR, Holmes C. Microglia in neurodegenerative disease. *Nature Reviews Neurology*. Apr 2010;6(4):193-201. doi:10.1038/nrneurol.2010.17
31. von Bernhardi R, Tichauer JE, Eugenin J. Aging-dependent changes of microglial cells and their relevance for neurodegenerative disorders. *Journal of Neurochemistry*. Mar 2010;112(5):1099-1114. doi:10.1111/j.1471-4159.2009.06537.x
32. Correale J. The role of microglial activation in disease progression. *Mult Scler*. Sep 2014;20(10):1288-95. doi:10.1177/1352458514533230

ACCEPTED MANUSCRIPT

Downloaded from https://academic.oup.com/braincomms/advance-article/doi/10.1093/braincomms/fcab301/6479693 by Turun Yliopiston Kirjasto user on 04 January 2022

33. Nutma E, Stephenson JA, Gorter RP, et al. A quantitative neuropathological assessment of translocator protein expression in multiple sclerosis. *Brain*. Nov 2019;142(11):3440-3455. doi:10.1093/brain/awz287
34. Nutma E, Ceyzériat K, Amor S, et al. Cellular sources of TSPO expression in healthy and diseased brain. *Eur J Nucl Med Mol Imaging*. Jan 2021;doi:10.1007/s00259-020-05166-2
35. Park C, Ponath G, Levine-Ritterman M, et al. The landscape of myeloid and astrocyte phenotypes in acute multiple sclerosis lesions. *Acta Neuropathol Commun*. 08 2019;7(1):130. doi:10.1186/s40478-019-0779-2
36. Zrzavy T, Hametner S, Wimmer I, Butovsky O, Weiner HL, Lassmann H. Loss of 'homeostatic' microglia and patterns of their activation in active multiple sclerosis. *Brain*. Jul 1 2017;140(7):1900-1913. doi:10.1093/brain/awx113
37. Elo P, Li XG, Liljenback H, et al. Folate receptor-targeted positron emission tomography of experimental autoimmune encephalomyelitis in rats. *Journal of Neuroinflammation*. Dec 2019;16(1)252. doi:10.1186/s12974-019-1612-3
38. Hagens MHJ, Golla SSV, Janssen B, et al. The P2X(7) receptor tracer C-11 SMW139 as an in vivo marker of neuroinflammation in multiple sclerosis: a first-in man study. *European Journal of Nuclear Medicine and Molecular Imaging*. Feb 2020;47(2):379-389. doi:10.1007/s00259-019-04550-x
39. Bagnato F, Hametner S, Yao B, et al. Tracking iron in multiple sclerosis: a combined imaging and histopathological study at 7 Tesla. *Brain*. Dec 2011;134(Pt 12):3602-15. doi:10.1093/brain/awr278
40. Hammond KE, Metcalf M, Carvajal L, et al. Quantitative in vivo magnetic resonance imaging of multiple sclerosis at 7 Tesla with sensitivity to iron. *Ann Neurol*. Dec 2008;64(6):707-13. doi:10.1002/ana.21582
41. Yao B, Bagnato F, Matsuura E, et al. Chronic multiple sclerosis lesions: characterization with high-field-strength MR imaging. *Radiology*. Jan 2012;262(1):206-15. doi:10.1148/radiol.11110601
42. Yao B, Ikonomidou VN, Cantor FK, Ohayon JM, Duyn J, Bagnato F. Heterogeneity of Multiple Sclerosis White Matter Lesions Detected With T2*-Weighted Imaging at 7.0 Tesla. *J Neuroimaging*. 2015 Sep-Oct 2015;25(5):799-806. doi:10.1111/jon.12193
43. Chawla S, Kister I, Wuerfel J, et al. Iron and Non-Iron-Related Characteristics of Multiple Sclerosis and Neuromyelitis Optica Lesions at 7T MRI. *AJNR Am J Neuroradiol*. Jul 2016;37(7):1223-30. doi:10.3174/ajnr.A4729
44. Haacke EM, Makki M, Ge Y, et al. Characterizing iron deposition in multiple sclerosis lesions using susceptibility weighted imaging. *J Magn Reson Imaging*. Mar 2009;29(3):537-44. doi:10.1002/jmri.21676
45. Absinta M, Sati P, Fechner A, Schindler MK, Nair G, Reich DS. Identification of Chronic Active Multiple Sclerosis Lesions on 3T MRI. *AJNR Am J Neuroradiol*. 07 2018;39(7):1233-1238. doi:10.3174/ajnr.A5660
46. Dal-Bianco A, Grabner G, Kronnerwetter C, et al. Long-term evolution of multiple sclerosis iron rim lesions in 7 T MRI. *Brain*. Jan 2021;doi:10.1093/brain/awaa436
47. Tolaymat B, Zheng W, Chen H, Choi S, Li X, Harrison D. Sex-specific differences in rim appearance of multiple sclerosis lesions on quantitative susceptibility mapping. *Mult Scler Relat Disord*. Oct 2020;45:102317. doi:10.1016/j.msard.2020.102317
48. Jang J, Nam Y, Choi Y, et al. Paramagnetic Rims in Multiple Sclerosis and Neuromyelitis Optica Spectrum Disorder: A Quantitative Susceptibility Mapping Study with 3-T MRI. *J Clin Neurol*. Oct 2020;16(4):562-572. doi:10.3988/jcn.2020.16.4.562
49. Yao Y, Nguyen TD, Pandya S, et al. Combining Quantitative Susceptibility Mapping with Automatic Zero Reference (QSM0) and Myelin Water Fraction Imaging to Quantify Iron-Related Myelin Damage in Chronic Active MS Lesions. *AJNR Am J Neuroradiol*. Feb 2018;39(2):303-310. doi:10.3174/ajnr.A5482

ACCEPTED MANUSCRIPT

Downloaded from https://academic.oup.com/braincomms/advance-article/doi/10.1093/braincomms/fcab301/6479693 by Turun Yliopiston Kirjasto user on 04 January 2022

50. Luchetti S, Fransen NL, van Eden CG, Ramaglia V, Mason M, Huitinga I. Progressive multiple sclerosis patients show substantial lesion activity that correlates with clinical disease severity and sex: a retrospective autopsy cohort analysis. *Acta Neuropathol*. 04 2018;135(4):511-528. doi:10.1007/s00401-018-1818-y
51. Prineas JW, Kwon EE, Cho ES, et al. Immunopathology of secondary-progressive multiple sclerosis. *Annals of Neurology*. Nov 2001;50(5):646-657. doi:10.1002/ana.1255
52. Harrison DM, Li X, Liu H, et al. Lesion Heterogeneity on High-Field Susceptibility MRI Is Associated with Multiple Sclerosis Severity. *AJNR Am J Neuroradiol*. Aug 2016;37(8):1447-53. doi:10.3174/ajnr.A4726
53. Elliott C, Belachew S, Wolinsky JS, et al. Chronic white matter lesion activity predicts clinical progression in primary progressive multiple sclerosis. *Brain*. Sep 1 2019;142(9):2787-2799. doi:10.1093/brain/awz212

ACCEPTED MANUSCRIPT

Downloaded from https://academic.oup.com/braincomms/advance-article/doi/10.1093/braincomms/fcab301/6479693 by Turun Yliopiston Kirjasto user on 04 January 2022

Figure legends

Figure 1. Flow chart of lesion phenotype analyses and illustrative MRI and PET images.

A. The flow chart illustrates the criteria for lesion inclusion and principles of the lesion classification. Lesion classification is based on proportions of active voxels in the lesion core and at rim. Rim-active lesions contain at least double the proportion of active voxels at the rim compared to core if 5 - 20 % of voxels in the core are active. Rim-active lesions have at least 5 %-point higher proportion of active voxels at the rim compared to the core, if less than 5 % of the voxels in the core are active. Inactive lesions have 0 % of active voxels in the core and at rim. Lesions which do not fit into the other two categories are classified as overall-active lesions. Of all included lesions 16 % were rim-active, 33 % were inactive and 51 % were overall-active. The DVR distribution of each lesion type is visualized with 3D surface plots.

B. T1 MR-image from an SPMS patient (top left) with corresponding parametric PET ^{11}C-PK11195 DVR images of the white matter (top middle) and the focal T1 lesions (top right). The bottom panel highlights the DVR values of selected lesions as 3D surface plots. The bottom row visualizes the voxels defined as active, with DVR > 1.56 (for more details, see the *methods* section). The colour bar of the PET images shows the dynamic range of DVR in the images.

Figure 2. Brain innate immune cell activation in multiple sclerosis patients and healthy controls.

Box plots of the ^{11}C-PK11195 DVR values representing the innate immune cell activation in the white matter of healthy controls and in the NAWM, and in association with lesions in the multiple sclerosis cohort. Wilcoxon rank-sum test was used for statistical analyses. In box plots the thick horizontal lines represent the medians, the boxes represent the IQR and the end of the whiskers or the points of the outliers represent the minimum and maximum values.

Figure 3. Association of volumetric parameters and innate immune cell activation with clinical disability.

Smaller brain (A) and NAWM volume (B) and larger T1 lesion load (C) associate with worse clinical disability measured with EDSS. Higher ^{11}C-PK11195 DVR in the NAWM associates with worse disability (D) and disease severity (E). In addition, higher radioligand binding in the perilesional area correlates with worse disability (F). Innate immune cell activation at lesion rim

ACCEPTED MANUSCRIPT

Downloaded from https://academic.oup.com/braincomms/advance-article/doi/10.1093/braincomms/fcab301/6479693 by Turun Yliopiston Kirjasto user on 04 January 2022

(G) or within T1 lesions (H) do not associate with EDSS. Here, ROIs encompassing the entire combined lesion volume or combined perilesional volume were evaluated.

Figure 4. Fractions of lesion types among multiple sclerosis subgroups

Proportions of the lesion subtypes differ between patients with EDSS < 4 and ≥ 4 (Fisher's exact test $P < 0.001$) (A) but not between RRMS and SPMS groups (B). Proportions of the lesion subtype volumes are different between patients with EDSS < 4 and ≥ 4 (Fisher's exact test $P < 0.001$) (C), and in RRMS vs. SPMS ($P < 0.001$) (D). The width of the bar represents the number of lesions (A and B) or lesion volumes (C and D) within the patient subgroup, and the height of the bar represents the percentage of the lesion type in question (A and B) or the volume percentage of the lesion type (C and D), with the exact percentage marked in the respective box. The total lesion numbers in the respective groups were: 1020 among patients with EDSS < 4 (69 patients) and 490 among patients with EDSS ≥ 4 (22 patients), 1020 among RRMS (67 patients), 490 among SPMS (24 patients). The total lesion volumes in the respective groups were: 251 cm^3 among patients with EDSS < 4 and 259 cm^3 among patients with EDSS ≥ 4, 240 cm^3 among RRMS and 269 cm^3 among SPMS.

Figure 5. Rim-active lesion load correlates with clinical disability and brain volume

The volume of rim-active lesions associates with higher clinical disability (A) and greater brain atrophy (B). The associations remain significant after multiple linear regression model.

Figure 6. Innate immune cell activation at rim is variable but more prevalent among patients with advanced disease

The number of active voxels at the rim was higher among secondary progressive compared to relapsing-remitting patients (A) and in patients with EDSS ≥ 4 compared to those with lower EDSS (B). The number of active voxels at rim correlated with EDSS-measured disability (C) and with MSSS-assessed disease severity (D). E demonstrates the great variability in both size and the degree of TSPO binding of rim-active lesions.

ACCEPTED MANUSCRIPT

Downloaded from https://academic.oup.com/braincomms/advance-article/doi/10.1093/braincomms/fcab301/6479693 by Turun Yliopiston Kirjasto user on 04 January 2022

Table 1 Demographic information and imaging parameters

		HC	MS	HC vs. MS	RRMS	SPMS	RRMS vs. SPMS	EDSS < 4	EDSS ≥ 4	EDSS < 4 vs. ≥ 4
Subjects	n	18	91		67	24		69	22	
Female	N_F	13	70	0.8	54	16	0.17	53	17	1
	%	72	77		81	67		77	77	
Age (y)	Mean	42.9	44.9	0.5	42.6	51.2	< 0.001	43.2	50.2	0.007
	SD	11.4	9.67		8.73	9.53		9.18	9.38	
Years since MS onset	Median		12.1		10.0	17.7	< 0.001	10.3	16.0	0.001
	IQR		7.25 - 15.8		6.55 - 13.8	12.5 - 22.9		6.64 - 13.8	12.3 - 22.7	
Disease modifying therapy*										
No therapy	n (%)		43 (47)		24 (36)	19 (79)	< 0.001	27 (39)	16 (73)	0.007
Moderate efficacy	n (%)		48 (53)		43 (64)	5 (21)		42 (61)	6 (27)	
NAWM volume (cm^3)	Mean	492	457	0.014	466	433	0.074	470	416	0.002
	SD	46.9	64.3		62.8	63.4		59.5	62.2	
NAWM volume (PF)	Mean	0.35	0.33	0.007	0.33	0.32	0.075	0.34	0.31	0.016
	SD	0.027	0.034		0.027	0.050		0.027	0.049	
Cortical GM volume (cm^3)	Mean	464	434	0.048	443	408	0.004	444	402	0.001
	SD	60.8	46.8		42.0	50.9		40.8	51.5	
Cortical GM volume (PF)	Mean	0.33	0.31	0.002	0.32	0.30	0.025	0.32	0.30	0.037
	SD	0.022	0.025		0.020	0.033		0.020	0.033	
T1 lesions > 27 mm^3	N_{T1}		1857		1215	642		1208	649	
..per patient	N_{T1}/n		20.4		18.1	26.8		17.5	29.5	
T1 lesion volume (cm^3)	Median		2.81		2.35	8.18	< 0.001	2.35	9.18	< 0.001
	IQR		1.48 - 7.60		1.17 - 4.30	4.35 - 17.5		1.20 - 4.26	4.53 - 18.2	
EDSS	Median		3.0		2.5	6.0	< 0.001	2.5	6.0	< 0.001
	IQR		2.0 - 3.5		2.0 - 3.0	3.9 - 6.5		2.0 - 3.0	5.1 - 6.5	
MSSS	Median		3.90		3.45	6.24	< 0.001	3.17	6.85	< 0.001
	IQR		2.39 - 5.20		2.24 - 4.74	3.81 - 8.13		2.15 - 4.74	4.35 - 8.1	

*Within 2 months prior the PET scanning. Gender and therapy comparison p-values are from Fisher's exact test. All other tests are Wilcoxon rank-sum test due to non-normality of the data. EDSS = expanded disability status scale, GM = grey matter, HC = healthy control, IQR = Interquartile range, MSSS = Multiple Sclerosis Severity Score, MS = multiple sclerosis, NAWM = normal appearing white matter, RRMS = relapsing remitting multiple sclerosis, SD = standard deviation, SPMS = secondary progressive multiple sclerosis

ACCEPTED MANUSCRIPT

Downloaded from https://academic.oup.com/braincomms/advance-article/doi/10.1093/braincomms/fcab301/6479693 by Turun Yliopiston Kirjasto user on 04 January 2022

Table 2 T1 lesions according to innate immune cell activation in various clinical MS subgroups

		All	RRMS	SPMS	RRMS vs. SPMS	EDSS < 4	EDSS ≥ 4	EDSS < 4 vs. ≥ 4
Number of patients, n		**91**	**67**	**24**		**69**	**22**	
Patients with rim-active lesions, n (%)		63 (69)	41 (61)	22 (92)		43 (62)	10 (91)	
Patients with inactive lesions, n (%)		85 (93)	65 (97)	20 (83)		67 (97)	18 (82)	
Patients with overall-active lesions, n (%)		87 (96)	64 (96)	23 (96)		66 (96)	21 (95)	
Average number of lesion subtypes per patient (median, IQR)	**Total**	**12 (7-22)**	**11 (7-20.5)**	**20 (10.5-36)**	**0.063**	**12 (7-20)**	**20.5 (9-34.25)**	**0.073**
	Rim-active	2 (0-4)	1 (0-3)	3 (1-4)	0.029	1 (0-3)	3 (1.25-6.5)	0.005
	Inactive	5 (2.5-7.5)	5 (3-7)	4 (1.75-8.25)	0.8	5 (3-7)	4 (1.25-7.75)	0.5
	Overall-active	6 (3-11.5)	6 (2-11)	10.5 (4.75-14.5)	0.051	6 (2-11)	11 (3.25-20.5)	0.033
Proportions of lesion subtypes per patient (%)	Rim-active	13 (0-21)	10 (0-20)	19 (11-26)	0.009	10 (0-20)	23 (12-28)	0.001
	Inactive	38 (21-56)	40 (23-61)	27 (12-46)	0.029	40 (24-60)	23 (12-41)	0.004
	Overall-active	48 (35-60)	47 (33-60)	51 (39-67)	0.3	45 (33-60)	52 (43-65)	0.11
Average lesion subtype volumes per patient (median, IQR)	**Total**	**2.21 (0.88-5.81)**	**1.77 (0.77-4.44)**	**7.20 (1.04-13.18)**	**< 0.001**	**1.77 (0.88-4.26)**	**7.92 (3.04-13.78)**	**< 0.001**
	Rim-active	0.13 (0-0.40)	0.06 (0-0.25)	0.41 (0.15-3.18)	< 0.001	0.06 (0-0.26)	0.47 (0.25-1.22)	< 0.001
	Inactive	0.40 (0.14-0.61)	0.41 (0.17-0.60)	0.26 (0.11-0.63)	0.5	0.40 (0.18-0.58)	0.25 (0.10-0.67)	0.5
	Overall-active	1.42 (0.29-5.81)	1.18 (0.22-3.44)	5.95 (2.51-8.76)	< 0.001	1.23 (0.22-3.89)	6.32 (1.93-8.78)	0.002
Proportions of lesion subtype volumes per patient (%)	Rim-active	4.3 (0-16)	2.4 (0-10)	13 (3.2-34)	0.001	2.4 (0-10)	13 (5.4-39)	< 0.001
	Inactive	18 (4.4-38)	23 (6.8-56)	4.9 (1.0-22)	0.002	23 (6.8-51)	4.3 (1.0-21)	0.003
	Overall-active	67 (43-83)	68 (40-82)	65 (50-86)	0.5	69 (41-84)	64 (46-81)	0.8
Average number of active voxels	Rim-active	92 (47-203)	74 (43-163)	158 (76-344)	0.022	73 (42-144)	210 (90-343)	0.003

Wilcoxon rank-sum test has been used to compare the groups due to non-normality of the data. All significant differences in comparisons remained significant after multiple comparison correction, using the false discovery rate method for the number of different tests in the groups being compared (n = 15). Lesion volumes in ml (cm^3), unless otherwise stated. Only white matter parts of the lesions with > 75 % of the volume in white matter are included. Only lesions with core and rim volumes > 27 cm^3 in white matter are included. Values are as median (IQR)

ACCEPTED MANUSCRIPT

Downloaded from https://academic.oup.com/braincomms/advance-article/doi/10.1093/braincomms/fcab301/6479693 by Turun Yliopiston Kirjasto user on 04 January 2022

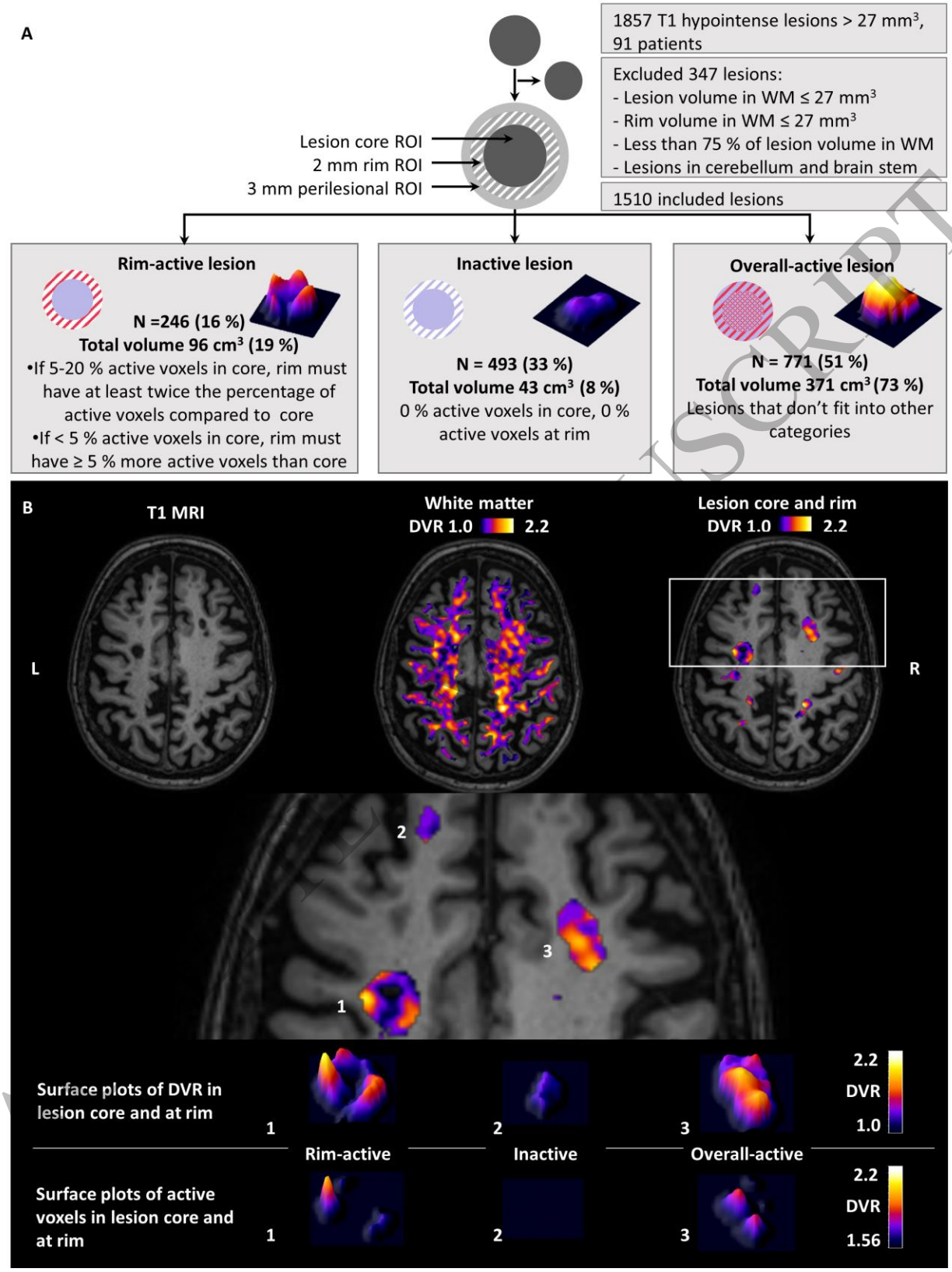

Figure 1
165x218 mm (0.2 x DPI)

Downloaded from https://academic.oup.com/braincomms/advance-article/doi/10.1093/braincomms/fcab301/6479693 by Turun Yliopiston Kirjasto user on 04 January 2022

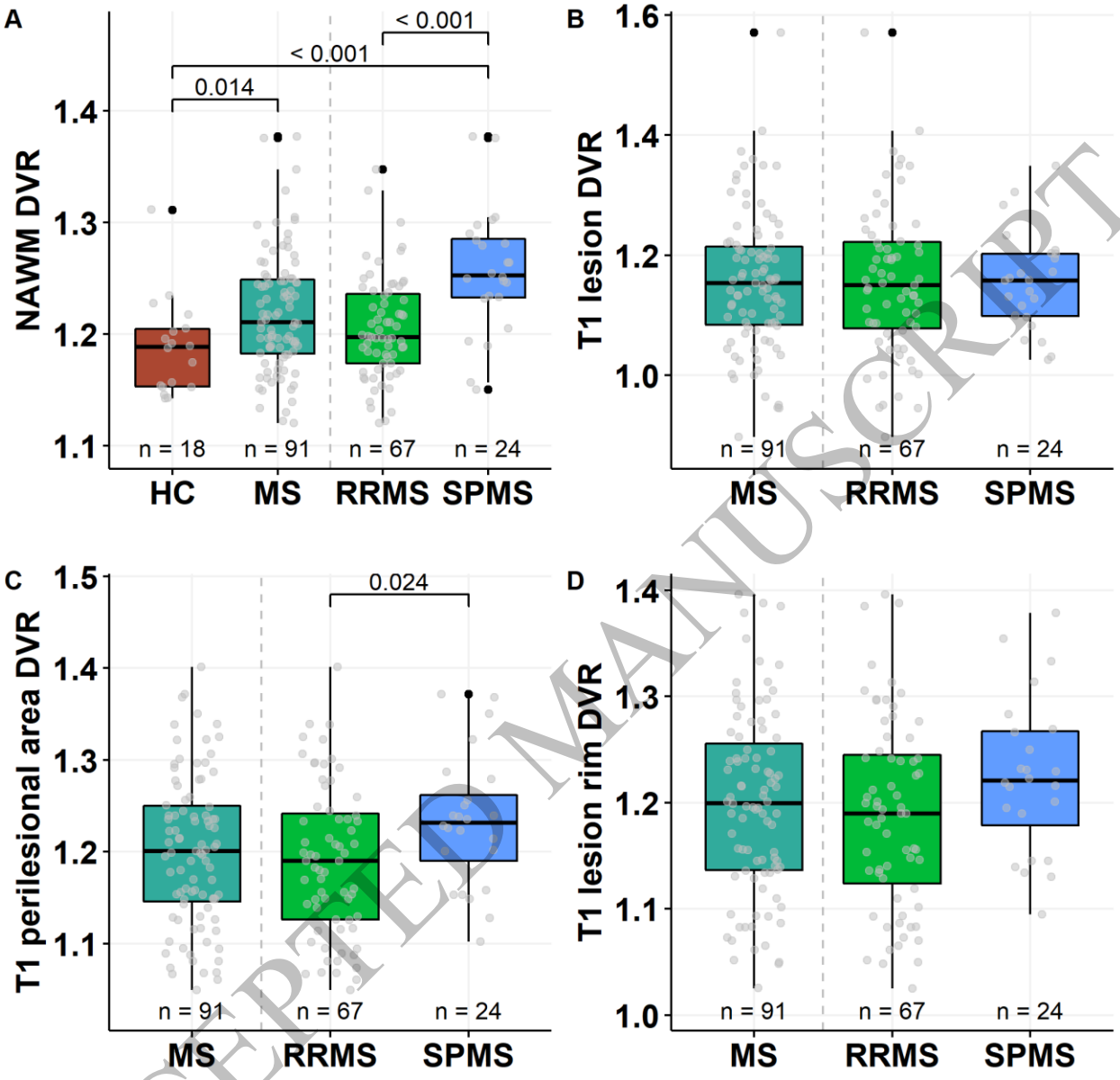

Figure 2
165x165 mm (0.2 x DPI)

ACCEPTED MANUSCRIPT

Downloaded from https://academic.oup.com/braincomms/advance-article/doi/10.1093/braincomms/fcab301/6479693 by Turun Yliopiston Kirjasto user on 04 January 2022

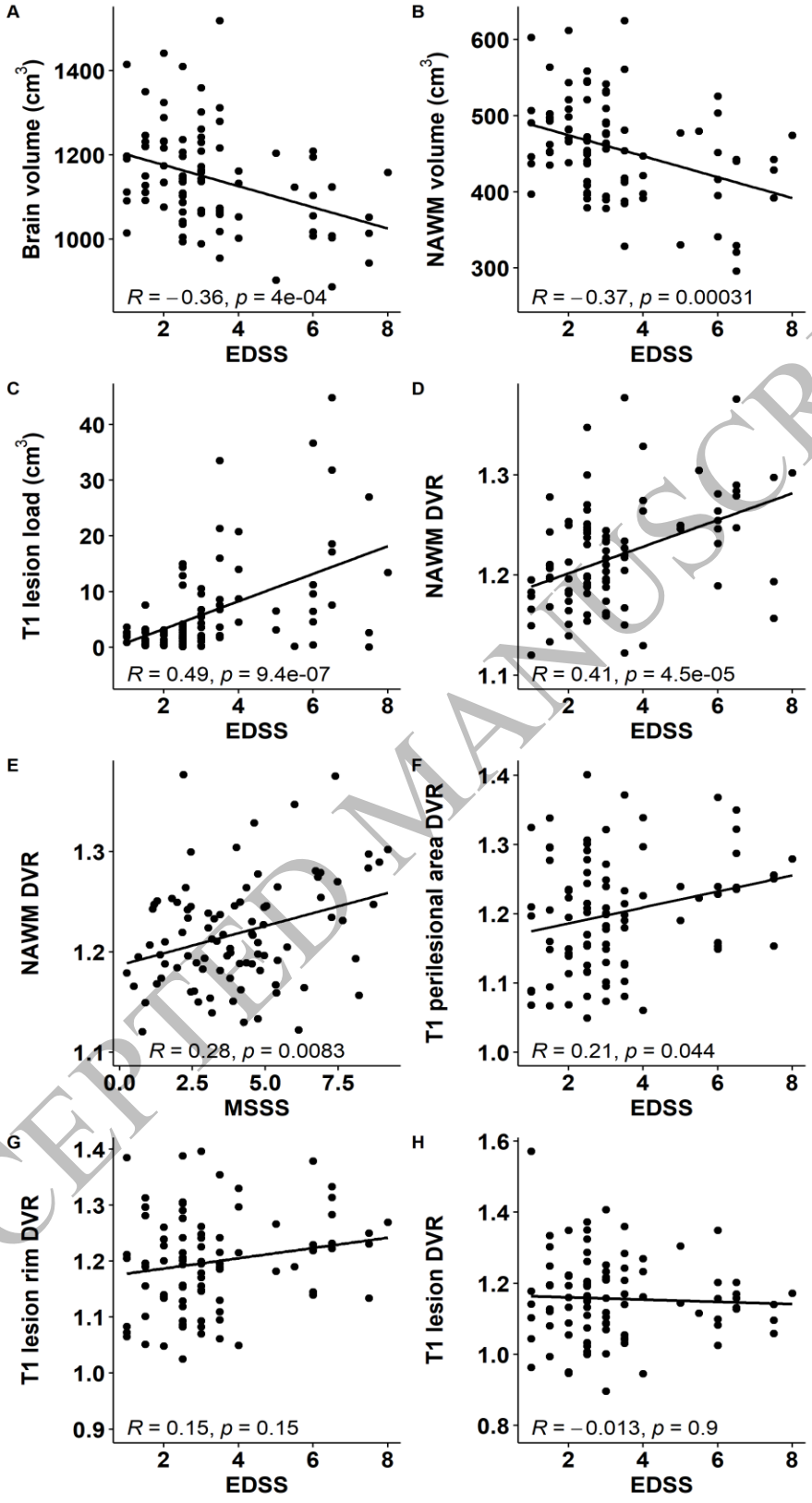

Figure 3
116x229 mm (0.2 x DPI)

ACCEPTED MANUSCRIPT

Downloaded from https://academic.oup.com/braincomms/advance-article/doi/10.1093/braincomms/fcab301/6479693 by Turun Yliopiston Kirjasto user on 04 January 2022

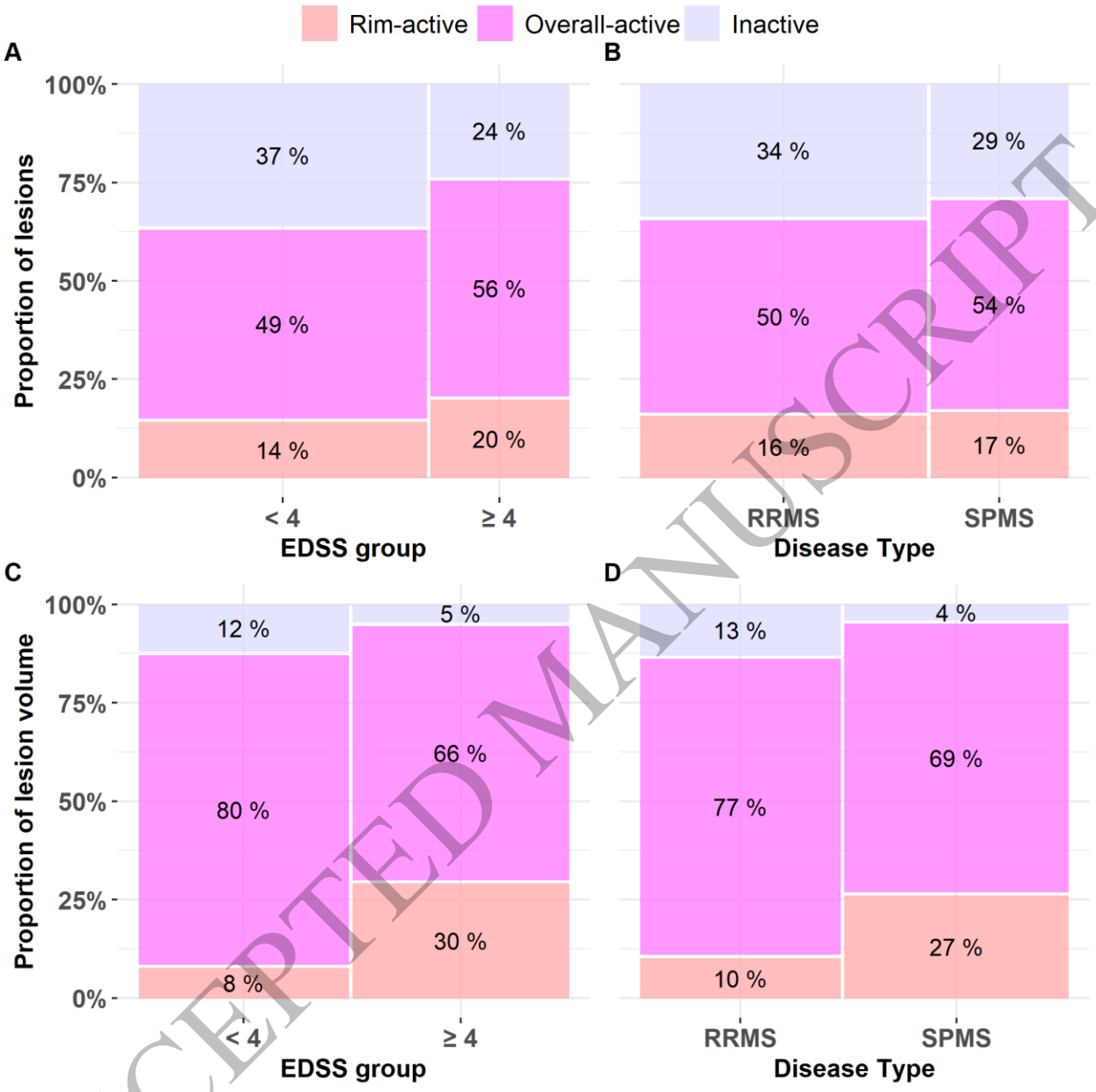

Figure 4
165x165 mm (0.2 x DPI)

ACCEPTED MANUSCRIPT

Downloaded from https://academic.oup.com/braincomms/advance-article/doi/10.1093/braincomms/fcab301/6479693 by Turun Yliopiston Kirjasto user on 04 January 2022

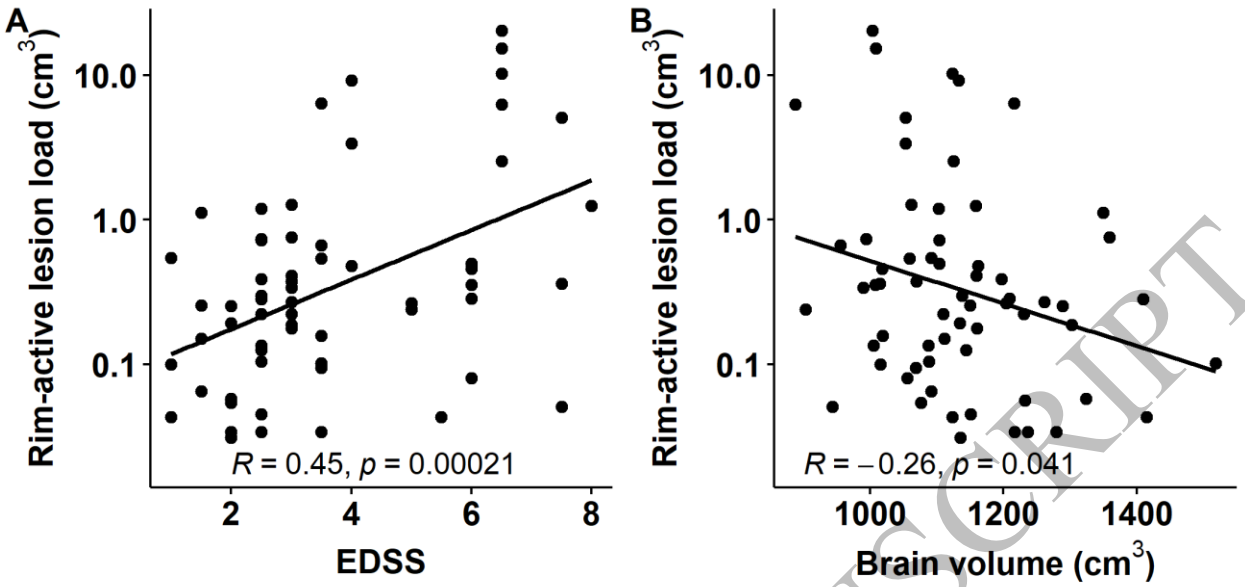

Figure 5
165x80 mm (0.2 x DPI)

ACCEPTED MANUSCRIPT

Downloaded from https://academic.oup.com/braincomms/advance-article/doi/10.1093/braincomms/fcab301/6479693 by Turun Yliopiston Kirjasto user on 04 January 2022

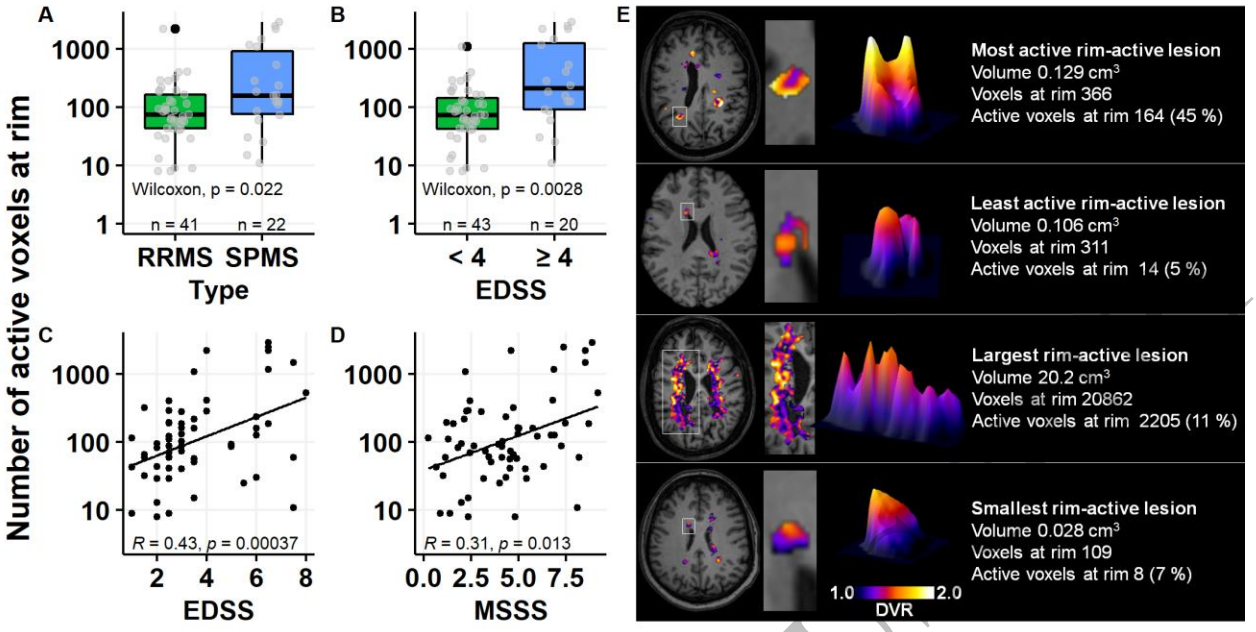

Figure 6
165x85 mm (0.2 x DPI)

ACCEPTED MANUSCRIPT

Downloaded from https://academic.oup.com/braincomms/advance-article/doi/10.1093/braincomms/fcab301/6479693 by Turun Yliopiston Kirjasto user on 04 January 2022

Brain Communications

BRAINCOM-2021-194

Abbreviated summary

This study describes in vivo phenotyping of multiple sclerosis lesions using TSPO-PET. Nylund et al. report that SPMS patients displayed high proportion of rim-active lesions, indicating greater innate immune cell activation at the chronic lesion edge. The methodology offers a new tool for individual assessment of smouldering MS lesion burden.

ACCEPTED MANUSCRIPT

Downloaded from https://academic.oup.com/braincomms/advance-article/doi/10.1093/braincomms/fcab301/6479693 by Turun Yliopiston Kirjasto user on 04 January 2022